

# DFT+U+J with linear response parameters predicts non-magnetic oxide band gaps with hybrid-functional accuracy

*D. S. Lambert<sup>a</sup> and D. D. O'Regan<sup>a\*</sup>*

a. School of Physics, SFI AMBER Centre and CRANN Institute, Trinity College Dublin, The University of Dublin, Ireland

## Abstract:

First-principles Hubbard-corrected approximate density-functional theory (DFT+U) is a low-cost, potentially high throughput method of simulating materials, but it has been hampered by empiricism and inconsistent band-gap correction in transition-metal oxides. DFT+U property prediction of non-magnetic systems such as  $d^0$  and  $d^{10}$  transition-metal oxides is typically faced with excessively large calculated Hubbard U values, and with difficulty in obtaining acceptable band-gaps and lattice volumes. Meanwhile, Hund's exchange coupling J is an important but often neglected component of DFT+U, and the J parameter has proven challenging to directly calculate by means of linear response. In this work, we provide a revised formula for computing Hund's J using established self-consistent field DFT+U codes. For non-magnetic systems, we introduce a non-approximate technique for calculating U and J simultaneously in such codes, at no additional cost. Using unmodified Quantum ESPRESSO, we assess the resulting values using two different DFT+U functionals incorporating J, namely the widely used DFT+(U-J) and the readily available DFT+U+J. We assess a test set comprising  $\text{TiO}_2$ ,  $\text{ZrO}_2$ ,  $\text{HfO}_2$ ,  $\text{Cu}_2\text{O}$  and  $\text{ZnO}$ , and apply the corrections both to metal and oxygen centered pseudoatomic subspaces. Starting from the PBE functional, we find that DFT+(U-J) is significantly outperformed in band-gap accuracy by DFT+U+J, the RMS band-gap error of which matches that of the hybrid functional HSE06.  $\text{ZnO}$ , a long-standing challenge case for DFT+U, is addressed by means of Zn 4s instead of Zn 3d correction, in which case the first-principles DFT+U+J band-gap error is half of that reported for HSE06.

## 1. Introduction

The electronic bandgap of a material is a property of high importance for semiconductor and photovoltaic applications. However, attempts to computationally model the bandgap using conventional Density Functional Theory (DFT) are consistently inaccurate[1]. This inaccuracy arises because the functionals used, such as the Local Density Approximation (LDA) and the Generalized Gradient Approximation (GGA), give rise to self-interaction error (SIE), among other systemic errors, leading to an underestimation of the band-gap. This can often be partially ameliorated through the use of hybrid functionals such as HSE06[2] and PBE0[3,4]. These functionals are often much more accurate at predicting band-gaps than purely local or semi-local DFT approximations, but can be much more computationally expensive depending on the

implementation and simulation size. This has motivated the search for, alongside others discussed in the recent review of Ref. [5], spatially localized corrections which act upon cost-effective semi-local DFT and which allow for accurate band-gap modelling without the need for hybrid-level computational costs[6-9].

Perhaps the most common correction applied to conventional DFT functionals is the Hubbard model inspired method now widely referred to as DFT+U[10-12], which in its simplest form effectively adds an energy penalty for partial occupation of pre-defined sets of localized orbitals. This method requires the choice of a value for the ‘U parameter’ to set the magnitude of the correction. The U value is often tuned to try and match experimental values, sometimes even those of quantities that are not ground-state DFT-accessible observables. This diminishes the first-principles nature of the DFT methodology and does not allow for the accurate prediction of gaps for less well-characterized or only theoretically predicted materials, where the band-gap values are necessarily not well known. In order to avoid the use of ad-hoc or empirical U values, several methods have been proposed for calculating the U value from first principles, such as the well-known finite-difference linear response method [13-15]. There, a U value is calculated in terms of the response of the occupancies of the aforementioned localized orbitals to an applied perturbation.

The use of DFT+U has faced many difficulties in properly modelling transition-metal oxide (TMO) band-gaps. The corrective terms of DFT+U are most commonly applied to pre-defined pseudo-atomic d orbitals of the metal ion(s) only, which can still result in a significant bandgap underestimation in  $d^0$  or  $d^{10}$  systems [16,17]. The application of DFT+U to metal orbitals alone also can result in a distortion of the geometric structure of the material[18-20]. It has become more common in recent years to apply U parameters to both the metal d-orbitals and the O 2p orbitals[21-27], however the U corrections calculated with linear response methods applied to all atoms have then tended to result in a band-gap overestimation[27]. In addition, attempts to calculate the U with linear response on non-magnetic oxides with nearly full or empty d orbitals such as ZnO have tended to fail, giving unreasonably high U values[23,28] or resulting in numerical instability in the calculations[29,30].

In addition to the Hubbard U correction, Hund’s J correction can also be incorporated in order to better account for the effect of intra-atomic exchange. Specifically, with Hund’s J in the present work we target spin-flip, or Hund’s 1st rule, exchange, and we refer the reader to Ref. [31] for a discussion of how different exchange terms relate to Hund’s 1st and 2nd rules. The incorporation of Hund’s exchange J into DFT+U has most conventionally been done through an “effective” U parameter, simply U-J, as established by Dudarev *et al.*[32], but there have been recent attempts to incorporate the J more comprehensively[33,34]. Himmetoglu *et al.*[35] proposed the use of a DFT+U+J functional with separately calculated U and J parameters. Linscott *et al.*[36], working within the minimum-tracking linear-response formalism, arrived at a factor-of-two smaller definition of Hund’s J required for consistency with the definition of the Hubbard U. This latter implementation has been shown to provide very accurate bandgaps for MnO[36] and TiO<sub>2</sub>[37]. In the present work, we combine the lessons of Refs. [35,36], calculating the Hund’s J using the conventional Self-Consistent Field (SCF) finite-difference linear-response approach as available in standard Quantum

ESPRESSO[38], but using the pre-factor for Hund’s J as required by consistency considerations as we proceed to explain.

The DFT+U+J functional can be easily incorporated into any code that already is already capable of DFT+U, and indeed several codes including Quantum ESPRESSO’s PWscf[39] and ONETEP[40] already support DFT+U+J. For non-spin-polarized systems, it is sufficient to use a DFT+U code to run DFT+U+J, as shown by Orhan *et al.*[37] and as we explain in section 2.1. Moreover, by taking this special case of the spin-polarized minimum-tracking linear-response framework proposed by Linscott *et al.*[36], it was found that the linear response U and J parameters can be computed simultaneously for non-spin-polarized systems. This method, termed here ‘the  $\gamma$ -method’, is described in the section 2.3 and is confirmed in the present study to work just as well within the well-known and long-established ‘SCF’ linear-response framework[13,14]. The  $\gamma$ -method is used extensively in the present work to calculate the Hund’s coupling J as an effectively cost-free by-product of Hubbard U calculations. To our knowledge, this represents the first successful demonstration of Hund’s J calculation by means of finite-differences density-functional linear-response theory.

While the DFT+U+J method is promising, it has not been evaluated on a large number of materials, as for example has recently been done for DFT+U with ortho-atomic orbitals by Kirchner-Hall *et al.*[27]. There has also been little investigation into whether the DFT+U+J methodology can introduce spurious geometric distortions into the lattice, as has been known to occur with other DFT+U techniques[18-20], and this also partially motivates the present work. In this study we have selected five representative  $d^0$  or  $d^{10}$  oxides as a challenging test set on which to benchmark and evaluate the DFT+U+J methodology against more common correction approaches. The materials chosen are  $\text{TiO}_2$ ,  $\text{ZrO}_2$ ,  $\text{HfO}_2$ ,  $\text{Cu}_2\text{O}$  and  $\text{ZnO}$ . These materials represent a range of different crystal structures, band-edge characters, and band-gap values, and have been previously studied extensively in experimental and computational literature.

In this study, U and J parameters are calculated using the first-principles SCF linear-response method for each of the test set materials. The resulting values are then used within DFT+U+J simulations to evaluate the effect of these corrections on band-gaps, effective masses, and cell geometries. These results are compared against longer-established methods such as the Perdew-Burke-Ernzerhof (PBE) functional[41], DFT+U and DFT+(U-J) based on a PBE starting point, as well as against hybrid-functional results from the literature. We find that DFT+U+J yields band-gap accuracies similar to hybrid functionals such as HSE06, on average, without causing spurious distortion of crystallographic or band-structure parameters.

## 2. Methodology

### 2.1 DFT+U+J functional corrections

The Hubbard U correction is an additional energy contribution that is used to approximately correct for the many-body self-interaction error (SIE), or more generally delocalization error, that is harbored within specific pre-defined subspaces in a practical local or semi-local DFT calculation. The DFT+U energy correction term takes the form of

$$E_U[\hat{n}^{I\sigma}] = \sum_{I\sigma} \frac{U^I}{2} \text{Tr}[\hat{n}^{I\sigma}(1 - \hat{n}^{I\sigma})], \quad (1)$$

where  $\hat{n}^{I\sigma}$  represents the projected Kohn-Sham occupancy matrix for spin  $\sigma$  and the subspace indexed  $I$ , and the  $U$  is an energy value that sets the magnitude of the correction. This reduces the degree of delocalisation by adding an energy penalty for non-integer occupancy matrix eigenvalues in the chosen subspace, which is spatially localized.

The  $U$  value can be selected by various methods, such as fitting to experiment, or reflecting past literature values. The linear response method, covered in the next section, allows for this value to be calculated from first-principles in situ for the material of interest, even self-consistently so[15], removing the reliance on empirical values.

Hund's  $J$  may be thought of as another correction parameter, on the same expansion order as the  $U$  and arguably a required counterpart to the  $U$ [36], which corrects for exchange effects that are ill-described by the approximate local or semi-local functional. The inclusion of  $J$  within DFT+ $U$ + $J$  tends to promote high-spin states[35], however the effect remains relevant to the energy and potential of ultimately non-spin-polarized systems[37]. Indeed, in the Hubbard Hamiltonian context, the Hund's exchange contribution may be separated into terms that are quadratic separately in the total density and spin density[42].

The  $J$  parameter is mostly commonly applied by combining  $U$  and  $J$  into a  $U$ - $J$  parameter, as in the formalism of Dudarev *et al.*[32]. In this method, which we will refer to as DFT+( $U$ - $J$ ), the  $J$  value is simply subtracted from the  $U$  value and implemented as an "effective  $U$ " of ( $U$ - $J$ ), giving

$$E_{U-J}[\hat{n}^{I\sigma}] = \sum_{I\sigma} \frac{U^I - J^I}{2} \text{Tr}[\hat{n}^{I\sigma}(1 - \hat{n}^{I\sigma})]. \quad (2)$$

However, there are also ways to implement the  $J$  correction separately, as an explicit term coupling unlike-spin densities. The DFT+ $U$ + $J$  functional[35] adds on a further term of the form (we neglect the 'minority term', as in that work and as is becoming customary)

$$E_J[\hat{n}^\sigma] = \sum_{I\sigma} \frac{J^I}{2} \text{Tr}[\hat{n}^{I\sigma} \hat{n}^{I-\sigma}], \quad (3)$$

where the  $J$  is an energy value that scales the magnitude of the exchange correction. This implementation was shown in Refs. [36] and [37] to provide accurate bandgaps with first-principles parameters for MnO and TiO<sub>2</sub>, respectively.

The DFT+ $U$ + $J$  functional can be activated directly using some codes such as Quantum ESPRESSO and ONETEP, but it can also be invoked in codes with no Hund's  $J$  implementation at all, in the specific case of non-spin-polarized systems[37], by using the

DFT+U code and the parameter substitution  $U_{full} = U - 2J$  applied simultaneously with a subspace potential shift of  $\alpha = J/2$ .

## 2.2 Linear response calculations of U and J

The total energy in subspace-perturbed DFT is given by

$$E = E_{\text{DFT}} + \alpha N + \beta M, \quad (4)$$

where N is given by  $N = n^\uparrow + n^\downarrow$ , where M is given by  $M = n^\uparrow - n^\downarrow$ , and where the  $n^\sigma$  are the traces of the perturbed subspace occupancy matrix of each spin.  $\alpha$  and  $\beta$  are the strengths of the subspace-uniform potentials that allow the occupancy N and magnetization M, respectively to be controlled at minimum energy cost, as guaranteed by the properties of the fully-relaxed constrained DFT energy landscape[43]. Here,  $\alpha$  is the strength of a perturbation that is the same for both spins. In the case of controlled magnetization M, the perturbation is repulsive with strength  $\beta$  for spin-up and attractive with strength  $\beta$  for spin down. Therefore,  $\beta$  is *half* of the difference in perturbation between the two spin channels, and we will recall this factor of one-half again presently.

To calculate U, a number of different  $\alpha$  potentials are applied, and the linear response of the occupation numbers gives the values for the bare (i.e., unscreened, or one-shot)  $\chi_0$  and the relaxed  $\chi$  subspace-projected linear response:

$$\chi_0 = \frac{dN_0}{d\alpha}, \chi = \frac{dN}{d\alpha} \quad (5)$$

Here,  $N_0$  is the total occupancy trace for the bare case. Fig. 1a) shows example calculations of  $\chi_0$  and  $\chi$ , with the slopes being calculated from least-squares linear regression. The U value can then be calculated [13,14] for on-site only DFT+U type corrections using the scalar equation:

$$U = \chi_0^{-1} - \chi^{-1} \quad (6)$$

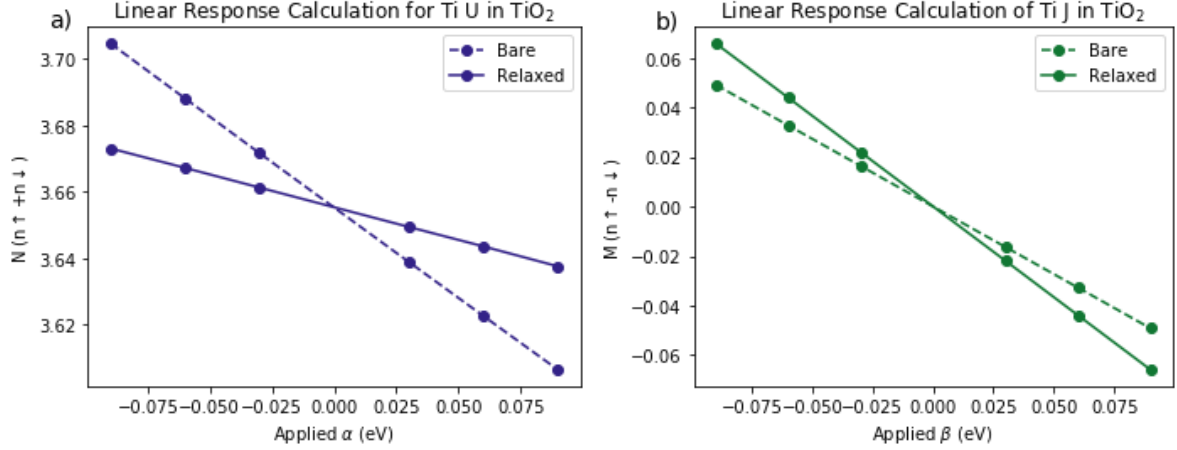


**Fig. 1. Example linear response calculations of a) the Hubbard U and b) Hund's exchange J for a pseudo-atomic Ti 3d orbital subspace in rutile TiO<sub>2</sub>.**

In order to see how this approach can be adapted to calculate the Hund's exchange coupling J, we base our definition on the ansatz for J for minimum-tracking linear response as defined in Eq. (22) of Linscott *et al.*[36], specifically

$$J = -\frac{1}{2} \frac{d(v_{\text{Hxc}}^{\uparrow} - v_{\text{Hxc}}^{\downarrow})}{d(n^{\uparrow} - n^{\downarrow})} \quad (7)$$

This formula measures the rate of change, with respect to subspace magnetization M, of subspace-averaged part of the interacting potential (Hxc denotes Hartree, exchange, and correlation) that applies to the magnetization density. This is akin, but technically different, to minus the second derivative of the interaction energy with respect to M, which would represent the global rather than subspace-specific analogue. Spurious energy-magnetization curvature is well associated with static correlation error in approximate density-functional theory, and we can interpret Hund's J as a measure of this, at least within the approximate subspace-bath decoupling and screening approximation of that underpins DFT+U type correction and linear response.

It is important to note at this point that this formula for J differs by a factor of one-half with respect to the similar formula proposed in Himmetoglu *et al.*[35], which was derived by analyzing the double-counting correction of the DFT+U+J functional introduced in that work, which substantially inspires the present one. The factor of one-half brings consistency with the Hubbard U as shown in Linscott *et al.*[36] (see Eqs. 20 and 24), by ensuring that the interacting analogue of the perturbation strength (the magnetization Lagrange multiplier β) is the potential that is being measured, and not twice that. Eq. (7) has recently used to calculate very accurate TiO<sub>2</sub> band-gaps from first-principles in Ref. [37]. The global minus sign is a matter of long-standing convention, e.g., from the Ising and Heisenberg Hamiltonians.

While this formula could, in principle, be directly used within self-consistent field DFT codes, in this work we explore instead its analogue within the long-standing approach used in those

codes for the non-interacting, bare response, namely that of evaluating perturbed occupancies before the interacting part of the potential begins to be updated. To see this, we first can rewrite

$$\begin{aligned}
J &= -\frac{1}{2} \frac{d((v_{\text{KS}}^{\uparrow} - v_{\text{ext}}^{\uparrow}) - (v_{\text{KS}}^{\downarrow} - v_{\text{ext}}^{\downarrow}))}{dM} & (8) \\
&= -\frac{1}{2} \frac{d(v_{\text{KS}}^{\uparrow} - v_{\text{KS}}^{\downarrow})}{dM} + \frac{1}{2} \frac{d(v_{\text{ext}}^{\uparrow} - v_{\text{ext}}^{\downarrow})}{dM} \\
&= -\frac{d\beta_{\text{KS}}}{dM} + \frac{d\beta}{dM} \approx -\frac{d\beta}{dM_0} + \frac{d\beta}{dM}.
\end{aligned}$$

Here,  $\beta_{\text{KS}}$  is the average of the spin-affecting Kohn-Sham potential over the subspace following the framework of Refs.[43,37], and the approximate equality signifies the relationship between minimum-tracking and SCF linear-response. In practice, notwithstanding, within self-consistent field codes such as Quantum Espresso, Abinit, CASTEP, VASP, and others, calculating the value for J from linear response involves calculating the bare and relaxed response of M to an applied  $\beta$ , as shown in Fig. 1b:

$$\chi_{M0} = \frac{dM_0}{d\beta}, \chi_M = \frac{dM}{d\beta}, \quad (9)$$

and J can ultimately be calculated, within the SCF linear-response formalism, as:

$$J = -\chi_{0M}^{-1} + \chi_M^{-1}. \quad (10)$$

We note that relaxation tends to enhance the magnetization response, in contrast to the occupancy response which is always reduced by screening (when perturbing from a stable state[43]). A positive value for the computed J indicates an erroneous effective magnetization-magnetization interaction within the subspace with a sign corresponding to underestimated Hund's exchange coupling in the underlying functional.

### 2.3 The $\gamma$ -method for simultaneous U and J calculation

Orhan and O'Regan[37] have demonstrated that within the minimum-tracking linear-response formalism and for non-spin-polarized systems, a simple procedure can be used to calculate both U and J simultaneously, using half the number of finite-difference calculations with respect to the usual method.

In calculations with both  $\alpha$  and  $\beta$  parameter, the  $\alpha$  parameter is applied equally to each spin, while the  $\beta$  parameter applies an opposite potential to each spin channel. In terms of the average values of the Kohn-Sham potential within the perturbed subspace[43], we have

$$V^{\uparrow} = V_{\text{DFT}} + \alpha + \beta, \quad (11)$$

$$V^{\downarrow} = V_{\text{DFT}} + \alpha - \beta. \quad (12)$$

If we set the value of  $\alpha$  to be equal to  $\beta$ , then the result is that a potential of  $2\alpha$  is applied to the spin-up channel alone, while the spin-down channel is unchanged. Setting  $\gamma=2\alpha$  for notational convenience, we can determine the spin-indexed response matrix[36] components from the trace of each individual spin channel occupancy matrix:

$$\chi^{\uparrow\uparrow} = \frac{d\text{Tr}[n^{\uparrow}]}{d\gamma} \quad (13)$$

$$\chi^{\downarrow\uparrow} = \frac{d\text{Tr}[n^{\downarrow}]}{d\gamma} \quad (14)$$

For a non-spin-polarized system, the remaining components of  $\chi$  are set by time-reversal symmetry:

$$\chi^{\uparrow\uparrow} = \chi^{\downarrow\downarrow} \quad (15)$$

$$\chi^{\downarrow\uparrow} = \chi^{\uparrow\downarrow} \quad (16)$$

These results together define the 2x2 response matrix  $\chi$ :

$$\chi = \begin{pmatrix} \chi^{\uparrow\uparrow} & \chi^{\uparrow\downarrow} \\ \chi^{\downarrow\uparrow} & \chi^{\downarrow\downarrow} \end{pmatrix} \quad (17)$$

This same procedure is separately used to determine the bare response  $\chi_0$ . The matrix difference between the inverted  $\chi$  and  $\chi_0$  matrices then yields the 2x2 interaction matrix  $f$ :

$$f = \chi_0^{-1} - \chi^{-1} \quad (18)$$

For ultimately non-spin-polarized systems where Eqs. (15,16) hold, the U and J values can then be derived from the elements of the resulting interaction matrix [36,37] as

$$U = \frac{f^{\uparrow\downarrow} + f^{\uparrow\uparrow}}{2} \quad (19)$$

$$J = \frac{f^{\uparrow\downarrow} - f^{\uparrow\uparrow}}{2} \quad (20)$$

Simplified into single scalar equations, and using the assumptions of Eqs. (15,16), the resulting equations become, in terms of the scalar quantities defined in Eqs. (13,14):

$$2U = (\chi_0^{\downarrow\uparrow} + \chi_0^{\uparrow\uparrow})^{-1} - (\chi^{\downarrow\uparrow} + \chi^{\uparrow\uparrow})^{-1} \quad (21)$$

And:

$$2J = (\chi_0^{\downarrow\uparrow} - \chi_0^{\uparrow\uparrow})^{-1} - (\chi^{\downarrow\uparrow} - \chi^{\uparrow\uparrow})^{-1} \quad (22)$$

An example of the calculations used to determine U and J with this method is shown in Fig. 2. Linscott *et al.*[36] have shown that within the minimum-tracking formalism, the calculated U and J from the scaled 2x2 methodology should match with  $\alpha$  and  $\beta$  method linear response U



and J calculations. Following this, Orhan *et al.*[37] utilized the efficiency brought by time-reversal symmetry to calculate minimum-tracking U and J values for both rutile and anatase TiO<sub>2</sub> with an LDA starting point. The exploitation of time-reversal symmetry for ultimately non-spin-polarized systems could, in principle, allow for the calculation of both U and J with as few as two  $\gamma$ -point simulations per subspace, although more points are used in this study to ensure that the resulting response is linear.

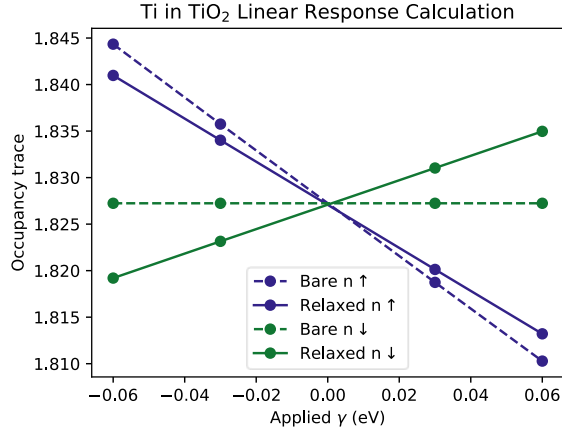


**Fig. 2. Example linear response calculation of U and J for a pseudo-atomic Ti 3d orbital subspace in rutile TiO<sub>2</sub>, using the  $\gamma$ -method and the standard Quantum Espresso package.**

Before leaving the theoretical methods behind, we emphasize that the  $\gamma$ -method is only applicable to non-spin-polarized systems. The same is true, even if  $\alpha$  and  $\beta$  are separately used, for Eqs. (19-22). For spin-polarized systems, the calculation of J requires the use of Eq. (10) directly, and ordinarily perturbing M using  $\beta$ .

## 2.4 Corrective functionals incorporating U and J

In this study, four different methods for incorporating the calculated U and J are considered and compared. The first method, referred to as DFT+U (metal only), takes the bare PBE simulation and adds the U correction to metal-atom centered nd subspaces alone, which is the most common application of U to TMOs. The quantum number n here is one less than the period in which the metal element resides. The correction is applied using Eq. (1). The second method, referred to as DFT+U (all atoms), applies the calculated U corrections to both metal nd and oxygen 2p subspaces, a practice that has been used in many recent studies[21-27].

The J parameter can be applied in different ways. The third method investigated involves subtracting the J value for each atom from the U value and applying this U-J value as the new U correction on all atoms, referred to as DFT+(U-J). The final method is that outlined by Linscott *et al.*[36], where the DFT+U+J functional of Eq. (7) and Ref. [35] is used to apply U and J corrections separately to metal and oxygen atoms, referred to here simply as DFT+U+J.

Each of these methods, alongside uncorrected PBE, are evaluated for their effect on the fundamental (generalized Kohn-Sham) band-gap, relaxed crystallographic parameters, and electronic band-structure of the test set materials, in order to determine whether they can accurately predict the bandgap of each material without causing distortions in other material parameters.

## 2.5 Computational details

The calculations in this study were conducted using the Quantum ESPRESSO package[38], utilizing the PBE exchange-correlation functional. For each element in every material, the charge neutral PSlibrary 1.0.0[44] ultrasoft pseudopotentials were used. The unit cell for each material was converged with respect to kinetic energy cut-off, charge density cut-off, and k-points, until the variable-cell relaxed energy difference was less than 1 meV per atom. Table 1 shows the converged unit cell parameters for each of the five materials. The energy and force convergence thresholds for relaxations were  $6 \times 10^{-5}$  Ry and  $10^{-4}$  Ry/Bohr respectively, a Fermi-Dirac smearing of 0.01 Ry was applied, and the Brillouin zone was sampled using a  $\Gamma$ -centered Monkhorst-Pack grid[45].

**Table 1: Converged simulation parameters for the unit cell of each of the five materials considered, meeting a 1 meV per atom convergence criterion.**

Material	Wavefunction Energy cut off (Ry)	Charge density energy cut-off (Ry)	k-point grid
TiO <sub>2</sub>	120	480	3x3x5
ZrO <sub>2</sub>	120	480	3x3x3
HfO <sub>2</sub>	130	520	3x3x3
Cu <sub>2</sub> O	60	240	5x5x5
ZnO	120	480	6x6x6

Before proceeding with calculations based on the  $\gamma$ -method, we first numerically verified its equivalence (for non-spin-polarized systems only) to the approach of separately using  $\alpha$  for U and  $\beta$  for J, using the non-supercell-converged unit cells of each of our test materials.

The first practical step in each case was to save the wavefunctions of a single-point SCF calculation using an energy convergence threshold of  $10^{-6}$  Ry. This was then restarted with the same initial wavefunction but with applied  $\alpha$  (for U calculations),  $\beta$  (for J calculations) potentials along with tighter convergence thresholds of  $10^{-11}$  Rydberg for the initial diagonalization and  $10^{-9}$  Ry total-energy convergence. The trace of the bare and relaxed occupancy matrices was extracted for several different applied potentials. Least-squares linear regression was used to determine  $\frac{dN}{d\alpha}$  and  $\frac{dM}{d\beta}$  and thus extract the appropriate  $\chi$  and  $\chi_0$  values to be used in Eq (6) (to calculate U) and Eq. (10) (to calculate J). The procedure for the  $\gamma$ -method

is similar, with a range of applied  $\gamma$  values being used to calculate  $\frac{dn}{d\gamma}$  for the spin-up and spin-down channels, and thus calculate the required  $\chi$  and  $\chi_0$  values that can be used to calculate U and J using Eqs. (21,22).

## 2.6 Effective mass calculations

The band-structure of each material between selected high-symmetry points was calculated in order to determine the location of the band-gap, and whether it is direct or indirect. In order to evaluate the effect of each method on the band-structure of the material, the scalar path-dependent effective mass was calculated from

$$m^* = \pm \hbar^2 \left( \frac{d^2E}{dk^2} \right)^{-1}. \quad (23)$$

The sign is positive when evaluating electron effective mass and negative when calculating hole effective mass. This was calculated from a parabolic fit at an appropriate energy range above or below the band edge for electrons and holes, respectively. The ranges in which a reliable parabolic fit was extracted were 0.05 eV for TiO<sub>2</sub>, HfO<sub>2</sub> and Cu<sub>2</sub>O; 0.01 eV for ZrO<sub>2</sub>, and 0.1 eV for ZnO.

## 3. Results

### 3.1 Verification and evaluation of the $\gamma$ -method

For the purposes of validating the  $\gamma$ -method, which halves the cost of calculating the parameter pair for non-spin-polarized systems, U and J values were calculated for the unit cell of each material. We compared the results given by the  $\alpha$  and  $\beta$  method of Section 2.2 and the  $\gamma$ -method of Section 2.3. Table 2 shows a comparison of the resulting values for rutile TiO<sub>2</sub>, which agree to within 0.5% of the U and J values calculated in the more obvious way, that is with  $\alpha$  for U and  $\beta$  for J.

**Table 2: Demonstration that the U and J values calculated for TiO<sub>2</sub> with the  $\alpha$  and  $\beta$  method of linear response and with the  $\gamma$ -method involving simultaneous U and J calculation are identical.**

Parameter	$\alpha$ and $\beta$ method (eV)	$\gamma$ -method (eV)	Difference (eV)	Difference (%)
Ti U	3.238	3.228	-1.087E-02	-0.336
Ti J	0.465	0.465	3.247E-04	0.070
O U	12.070	12.035	-3.519E-02	-0.292
O J	1.826	1.835	8.823E-03	0.483

Similar tables for the other four materials are collected in Appendix I. For all atomic elements of all materials, there is less than 1% difference between the U and J calculated using the methods, indicating that that the  $\gamma$ -method is equivalent to the  $\alpha$  and  $\beta$  method for ultimately

non-spin-polarized systems. In Ref. [36], this was confirmed to be the case also within the minimum-tracking linear response definitions of  $U$  and  $J$ . By using the  $\gamma$ -method, when spin polarization is not anticipated, the calculation of Hund’s coupling  $J$  can be performed as an essentially cost-free by-product of calculating the Hubbard  $U$ , using Eqs. (21,22). Thus, it is encouraging to confirm its validity here for the SCF (standard) linear-response calculations now very routinely performed using plane-wave DFT codes.

### 3.2 Rutile TiO<sub>2</sub> results

The linear response  $U$  and  $J$  values for rutile TiO<sub>2</sub> were calculated using different supercell sizes, as shown in Table 3. These parameters were performed for the Ti 3d and O 2p orbitals separately, as motivated by previous studies [25-27,37,46,47]. At acceptable convergence of the derived quantities that these parameters will be used to calculate, the supercell calculations ultimately agree to within 0.04 eV for all parameters. The calculated  $U$  values for Ti and O are within the range of previous linear response studies[25,27,37]. It should be noted that different population analysis schemes for defining the DFT+ $U$  subspaces can yield significantly different calculated  $U$  parameters and subsequent results[27,48]. In this study the DFT+ $U$  population analysis uses the default, neutral-configuration non-orthonormalized pseudo-orbitals generated by PWscf. The  $U$  and  $J$  values for the largest supercell size of 3x3x5 was used for the materials property calculations that follow.

**Table 3: Convergence of calculated linear response  $U$  and  $J$  values for Ti 3d and O 2p subspaces in rutile TiO<sub>2</sub> with different supercell sizes and k-point grids.**

Supercell size	k-points	Ti $U$ (eV)	Ti $J$ (eV)	O $U$ (eV)	O $J$ (eV)
unit cell	5x5x8	3.228	0.465	12.035	1.835
2x2x3	$\Gamma$ -point	3.238	0.383	11.214	1.679
2x2x3	2x2x2	3.240	0.385	11.237	1.682
3x3x5	$\Gamma$ -point	3.225	0.384	11.199	1.688

Experimentally, the fundamental band-gap of rutile TiO<sub>2</sub> has been measured to be 3.03 eV by very-high-resolution absorption[49] and time-integrated photoluminescence[50]. Fig. 3a) shows a comparison of rutile TiO<sub>2</sub> bandgaps derived from experiment, from hybrid and GW techniques, and from the methods examined in this study. The average HSE06 bandgap value[49,50] is the closest of the hybrid methods, with a slight bandgap overestimation of 0.24 eV, while PBE0 values[51,52] found in the literature overestimate the gap by an average of 0.92 eV, and even  $G_0W_0$  methods[53,54] overestimate by 0.37 eV. Our PBE value with no corrections applied greatly underestimates the experimental gap by 1.19 eV, and applying DFT+ $U$  to the Ti 3d subspace alone does not significantly improve this, in agreement with previous studies[27,37,47]. When the  $U$  is applied to both Ti and O, however, the bandgap is increased and becomes 0.80 eV larger than the experimental one.

Incorporating Hund’s exchange coupling  $J$  as well as  $U$  brings the calculated bandgap back down. In the case of the DFT+( $U$ - $J$ ) method, there is still an overestimation of 0.39 eV, while

the DFT+U+J functional is the most accurate of those tested, giving an underestimation of 0.24 eV. This echoes the recent findings for rutile in Ref. [37], albeit that a significantly better agreement with experiment was found there with an LDA rather than a PBE starting point, and with charge-neutral LDA pseudo-atomic orbitals defining the subspaces. The zero-point phonon correction is expected to be negligible in rutile[55], with respect to the band-gap inaccuracies in question here. The DFT+U+J bandgap error here is lower than both PBE0 and  $G_0W_0$  methods and is equal to the HSE06 average error, but with a significantly lower computational cost and indeed minor extra cost over PBE after the U and J parameters are calculated.

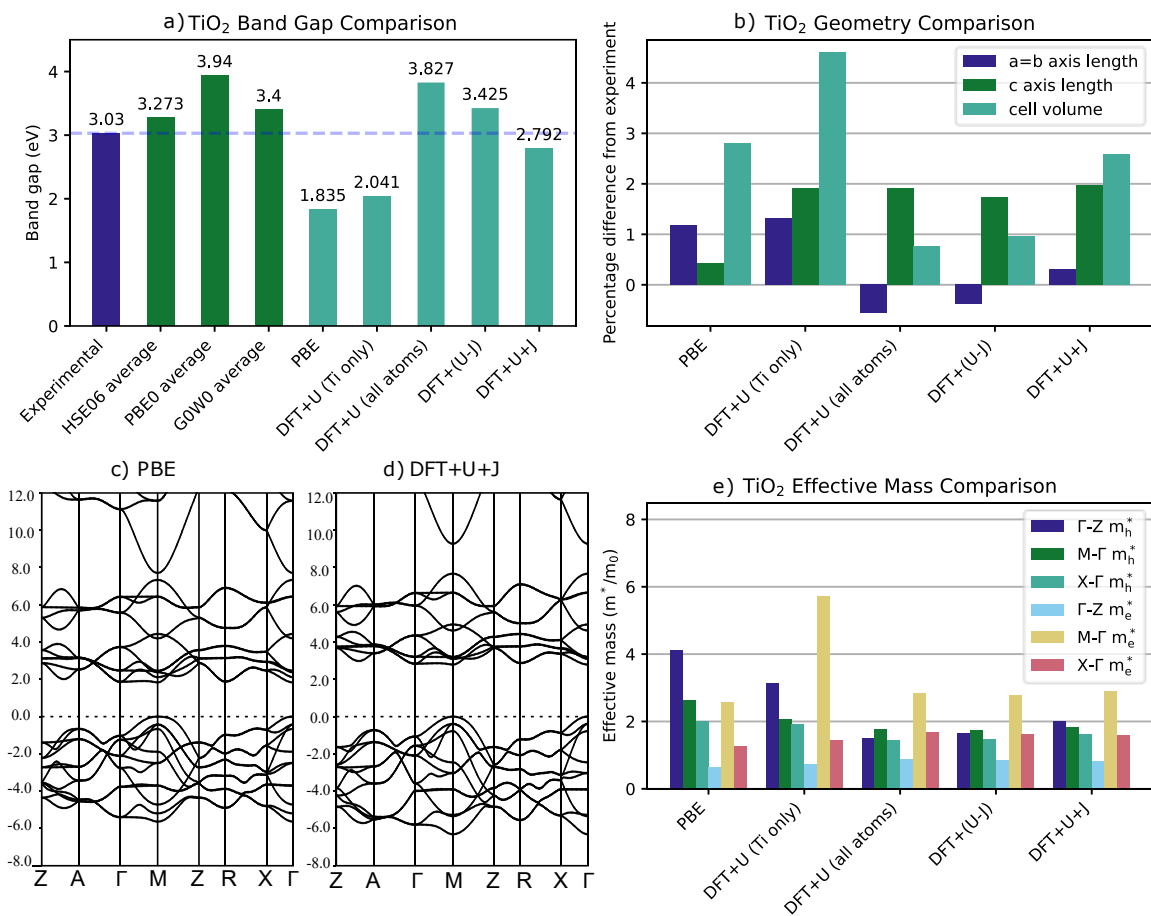


**Fig. 3. Summary of effect of different U and J incorporating corrective functionals on rutile TiO<sub>2</sub> material properties. a) Comparison of the experimental rutile bandgap[49,50] with an average of literature bandgap values for HSE06[54,56,57], PBE0[51,52], and  $G_0W_0$ [53,54], and with the five PBE-derived functionals utilizing U and J parameters. b) Percentage deviation of crystallographic parameters (axis lengths and volume) from experimental values for each correction method. c) The band-structure of rutile for the PBE functional with no corrections applied. d) The band-structure of rutile using the DFT+U+J functional. e) Calculated effective mass ratios in selected directions for the five functionals.**

Fig. 3b. shows the effect of the methodologies on the axis lengths and volume of the cell, as a percentage of the experimental value. Applying the +U on the Ti 3d orbitals results in a stretching of the c-axis, increasing the volumetric error by around 2%. Applying DFT+U on both the Ti 3d and O 2p orbitals maintains the c-axis stretching, but shrinks the a and b axes to below the experimental value, resulting in a volumetric error that is smaller than that of uncorrected PBE. Applying U and J, both to Ti 3d and O 2p subspaces results in an a=b axis length very close to experiment, but slightly increases the volumetric error. Overall, apart from the U on Ti 3d only case, no methodology results in a significantly distorted geometry with respect to either experimental or PBE values. This is reminiscent of the findings in Linscott *et al.*[36], where it was shown that the O 2p counterpart correction cancels the tendency for metal 3d correction to over-elongate bonds in hydrated metal complexes.

There is similarly little band-structure distortion arising from the DFT+U+J methodology. Fig. 3c. and Fig. 3d. depict the band-structures for bare PBE and for the full DFT+U+J methodology. There does not appear to be a large structural difference in the band-structure near the gap, apart from the greater bandgap, with both methods predicting a direct bandgap with the conduction-band minimum (CBM) at the  $\Gamma$  point, only slightly lower in energy than the CBM at the M point. This difference is 32 meV for PBE and 45 meV for DFT+U+J. The bandwidth of the valence band is also increased from 5.6 eV for PBE to 6.3eV for DFT+U+J.

Fig. 3e. shows how the calculated effective mass of electrons and holes were affected by the corrective functionals. The application of DFT+U tends to decrease the effective mass of holes, with the largest effect occurring in the  $\Gamma$ -Z direction. The effective mass of electrons is increased when U is applied, and this is most prominently seen along the M- $\Gamma$  direction for the DFT+U (Ti only) method, although this may be an artifact of the very flat band-structure along this direction. The U corrections also appear to have the effect of making the band-structure of the holes more isotropic, bringing the effective mass parameters closer to each other. It can be seen that the two functionals incorporating J yield a band-structure that is almost identical to that of DFT+U(all atoms), indicating that the J corrections have little effect on the rutile band-structure, except for the gap. These latter variations, while interesting, are difficult to base assessment upon, given that experimental estimations of the electron effective mass in rutile can vary by an order of magnitude[58,59].

### 3.3 Monoclinic ZrO<sub>2</sub> results

The two O atoms in the ZrO<sub>2</sub> formula unit are subject to two different chemical environments, with one O atom being 3-fold coordinated and another being 4-fold coordinated. As a result, different U and J values can be calculated and applied to each of the O atoms[27]. Table 4 shows the convergence of calculated U and J parameters for ZrO<sub>2</sub> for Zr and the two different O environments. The values from the largest supercell are used in this study.

**Table 4: Convergence of calculated U and J parameters for ZrO<sub>2</sub> for different supercell sizes and k-point grids. The U and J values were calculated separately for the Zr 4d subspace, 3-fold coordinated O atom 2p subspaces, and 4-fold coordinated O atom 2p subspaces.**

Supercell size	k-points	Ti U (eV)	Ti J (eV)	O 3-fold U (eV)	O 3-fold J (eV)	O 4-fold U (eV)	O4-fold J (eV)
unit cell	3x3x3	1.724	0.346	14.126	2.342	15.665	2.564
2x2x2	$\Gamma$ -point	1.735	0.337	14.277	2.317	15.590	2.559
2x2x2	2x2x2	1.740	0.336	14.250	2.327	15.590	2.532
3x3x3	$\Gamma$ -point	1.736	0.338	14.277	2.339	15.453	2.564

Fig. 4a. shows the effect of U and J on the crystallographic geometry error. The PBE volumetric error is increased slightly when DFT+U is applied to Zr 4d subspaces alone, but when a U value is applied to the O atoms as well, the volumetric error decreases well below the PBE value, due to an underestimation of the b-axis size cancelling out slight overestimations of the a and c axes. In the case of U and J, the b axis length and  $\beta$  angle match almost exactly with experimental values, but the a and c axis lengths are larger, leading to a volumetric error that is about the same as in uncorrected PBE simulations. This indicates that, aside from the most commonly used DFT+U approach of targeting Zr 4d orbitals only, no methodology distorts the ionic geometry significantly.

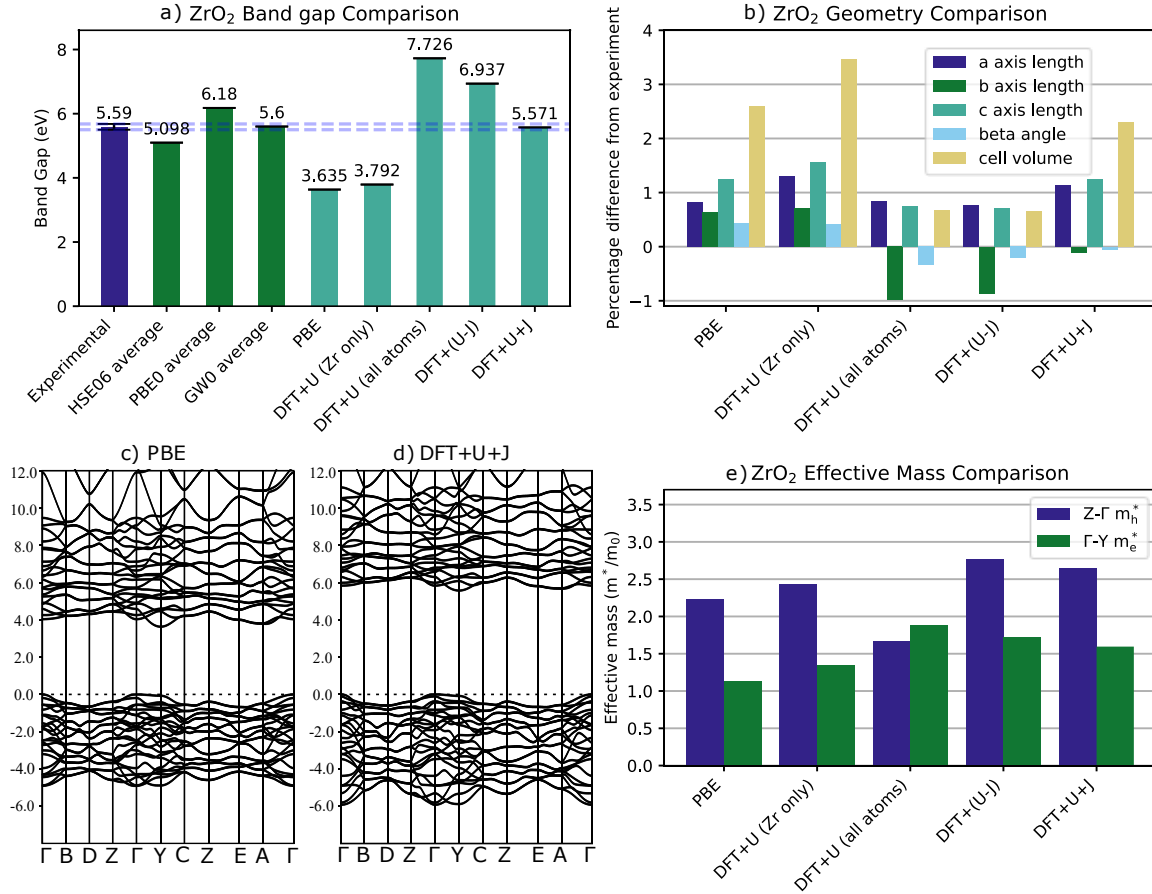


**Fig. 4. Summary of effect of different U and J incorporating corrective functionals on ZrO<sub>2</sub>, showing: a) The effect of methodology on band-gap, compared to experiment and the literature values for HSE06[60-63], PBE0[64,65] and GW0[66-68]. b) The effect of methodology on unit cell geometries, as a percentage difference from the experimental values[69,70]. c) The band-structure for PBE. d) The band-structure for DFT+U+J e) Comparison of calculated effective mass values along selected directions.**

Fig. 4c. and Fig. 4d. show the band-structures calculated using the PBE and DFT+U+J functionals, which are qualitatively very similar apart from the differing bandgaps. The effective mass of the electrons and holes are slightly increased when U and J are applied, but the results are not significantly different from PBE values. As with rutile TiO<sub>2</sub>, there is an expansion of the valence band width, from 4.9 eV for PBE to 5.9 eV DFT+U+J.

Overall, the first-principles DFT+U+J approach seems to be highly efficient at correcting the band-gap to the experimental value without distorting geometry or band-structure. This negates the pre-supposition that DFT+U methods are fundamentally inapplicable to d<sup>0</sup> or d<sup>10</sup> systems. We emphasize that both Hund's coupling J and oxygen 2p terms are needed for satisfactory results, for different reasons.



### 3.4 Monoclinic HfO<sub>2</sub> results

Monoclinic HfO<sub>2</sub> is similar to ZrO<sub>2</sub> in that it comprises 3-fold and 4-fold coordinated O atoms that yield different calculated U and J values. Table 5 shows the convergence behavior of these parameters. The U and J values for the largest supercell are used.

**Table 5: Convergence of calculated U and J parameters for HfO<sub>2</sub> for different supercell sizes and k-point grid parameters. The U and J values were calculated separately for Hf 5d subspaces, 3-fold coordinated O atom 2p subspaces, and 4-fold coordinated O atom 2p subspaces.**

Supercell size	k-points	Hf U (eV)	Hf J (eV)	O U 4-fold (eV)	O J 4-fold (eV)	O U 3-fold (eV)	O J 3-fold (eV)
unit cell	3x3x3	1.442	0.327	17.875	3.139	16.071	2.863
2x2x2	$\Gamma$ -point	1.443	0.321	17.755	3.092	16.350	2.811
2x2x2	2x2x2	1.438	0.324	18.065	3.115	16.251	2.819
3x3x3	$\Gamma$ -point	1.441	0.323	17.815	3.144	16.187	2.829

Similarly to the case of ZrO<sub>2</sub>, the experimental gap of HfO<sub>2</sub> is not well known. We again use an average of IPES studies to estimate the fundamental bandgap as 5.78 eV[69,70]. Fig 5a. shows that G<sub>0</sub>W<sub>0</sub> calculations in the literature have yielded values that match within 0.01 eV of this value, with GW<sub>0</sub> results slightly overestimating it by 0.28 eV. As is the case with TiO<sub>2</sub> and ZrO<sub>2</sub>, the PBE0 functional overestimates the band-gap (by 0.73 eV), while the HSE06 result is much closer (within 0.09 eV). In our simulations, the PBE functional underestimated the band-gap by 1.58 eV, with the underestimation only improving to 1.46 eV when the DFT+U correction was applied to Hf 5d subspaces alone. Applying U to both O 2p subspaces results in a very large bandgap overestimation of 3.37 eV, which is slightly reduced to 2.42 eV by the Dudarev DFT+(U-J) functional. The PBE+U+J approach once again yields the most accurate bandgap of the cost-effective PBE-derived approaches, with an overestimation of 0.61 eV, which is more accurate than PBE0 for this system but falls short of the HSE06 performance.

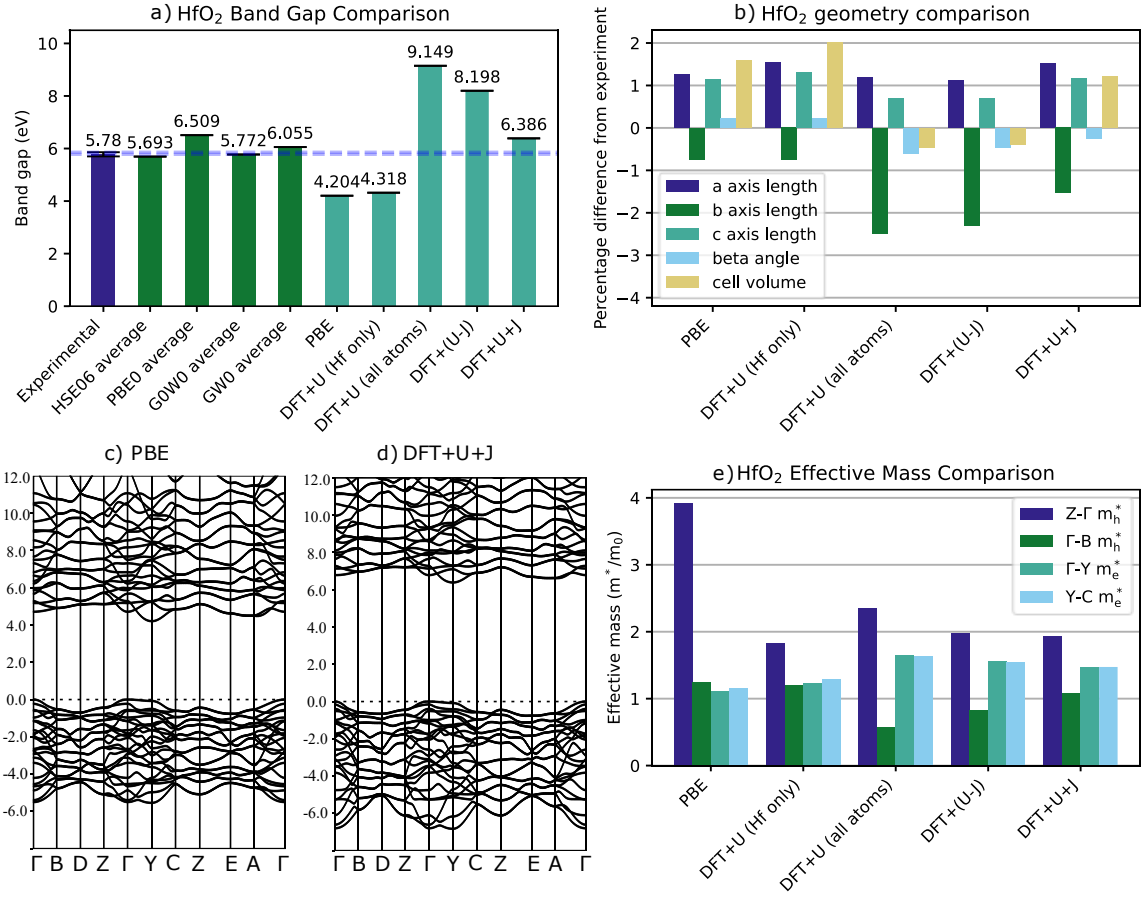


**Fig. 5. Summary of effect of different U and J incorporating corrective functionals on HfO<sub>2</sub> material properties, showing: a) Calculated bandgaps from different methodologies, compared to experiment[69,70], HSE06[71-73], PBE0[71,74,75], GoW0[67,76,77], and GW0[66,67,76]. b) Difference with respect to experiment values for crystallographic cell properties and total volume for each method. c) Band-structure from uncorrected PBE. d) Band-structure from the first-principles DFT+U+J method. e) Effective mass of electrons and holes along selected directions for each functional.**

The geometric effect of the various U and J methods on HfO<sub>2</sub> is shown in Fig 5b. The application of U has a small stretching effect on the a and c axes, resulting in a slight increase in volumetric distortion. Applying the U additionally to the O atoms rectifies this somewhat, and also results in a large degree of shrinkage in the b-axis, resulting in a low volumetric error. The application of J reduces this shrinkage but increases the a-axis and b-axis lengths, resulting in a volumetric error that is ultimately slightly lower than the case of uncorrected PBE. Fig 5c. and Fig 5d. shows the band-structure of uncorrected PBE and DFT+U+J based on PBE, showing that there is not a large amount of change between them. Fig 5e. shows the resulting effect on effective mass. The application of the corrective functionals tends to increase the effective mass of electrons slightly. The hole effective mass is reduced, conversely, but since

the lines are very flat it is difficult to assess the difference. As is the case for TiO<sub>2</sub> and ZrO<sub>2</sub>, the valence band width is increased, now from 5.5 eV for PBE to 6.8 eV for DFT+U+J.

### 3.5 Cubic Cu<sub>2</sub>O results

The convergence of calculated U and J parameters is shown in Table 6, indicating a reasonable degree of convergence with the accessible supercell sizes. The band-gap of Cu<sub>2</sub>O was found by an IPES study to be 2.17[78]. Fig. 6a. shows the band-gaps of different methods compared to this result. Hybrid PBE0 modelling has overestimated the band-gap by 0.30 eV, while HSE06 models have slightly underestimated the bandgap by 0.24 eV.

**Table 6: Convergence of calculated U and J parameters for Cu and O atoms in cubic Cu<sub>2</sub>O with different supercell sizes and k-point sampling.**

Supercell size	k-points	Cu U (eV)	Cu J (eV)	O U (eV)	O J (eV)
2x2x2	Γ-point	12.382	1.850	20.358	3.199
2x2x2	3x3x3	12.450	1.961	20.801	3.183
3x3x3	Γ-point	12.525	1.933	20.601	3.168
3x3x3	2x2x2	12.537	1.960	20.551	3.188
4x4x4	Γ-point	12.526	1.958	20.240	3.203
5x5x5	Γ-point	12.476	1.954	20.407	3.191

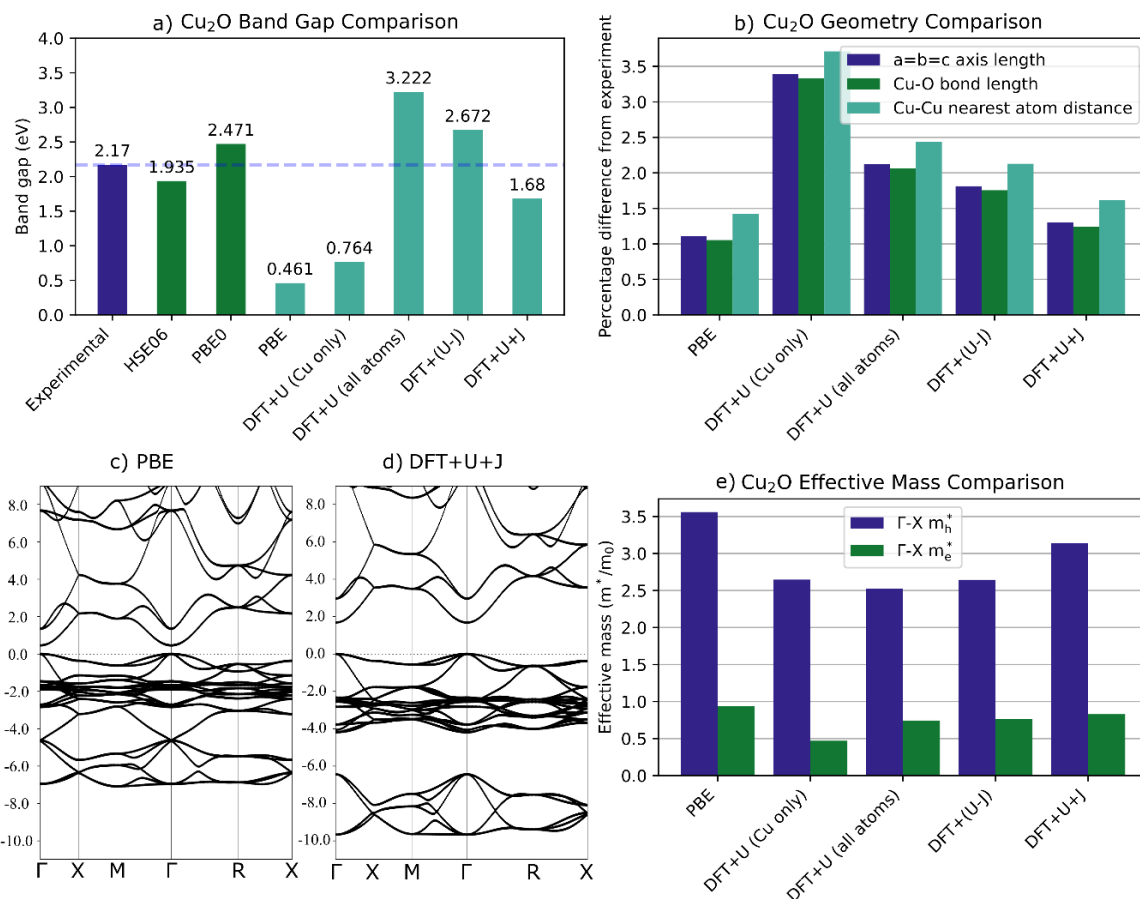


**Fig. 6. Summary of effect of different U and J incorporating corrective functionals on Cu<sub>2</sub>O material properties. a) Comparison of predicted bandgaps for the five functionals with the experimental value,[78] as well as an average of HSE06 literature values[17,79-83] and PBE0 values[17,82,84]. b) Percentage deviation of crystallographic properties (axis and inter-atomic distances) from experimental values for each method. c) PBE band-structure with no corrections applied. d) PBE structure with both U and J corrections applied to Cu and O. e) Effective mass in selected directions for the five functionals.**

Our calculated band-gap with PBE and no corrections greatly underestimates the band-gap by 1.71 eV. Applying the first-principles U value to the Cu 3d orbitals alone only lessens the overestimation to 1.41 eV. Applying the U to both the Cu and O atoms again results in an overestimation of the band-gap value, by 1.05 eV, which can be reduced by DFT+(U-J) to 0.50 eV. This is very similar to the final error of 0.49 eV for the DFT+U+J method, which instead errs the side of underestimation. DFT+U+J is again the best performing of the PBE-based functionals but falls short of the hybrid accuracy in this case.

The effect of corrective functional on crystallographic parameters is shown in Fig. 6b. The PBE geometry is quite accurate, with values that are within 1.5% of experimental values. Applying the DFT+U correction to the Cu 3d subspaces alone introduces some distortions, with cell

parameter errors rising to about 3.5%. These distortions decrease back down to around 2% for DFT+U (all atoms) and DFT+(U-J). The DFT+U+J method reduces the errors still further, and turns out to be almost as good as uncorrected PBE. This indicates that DFT+U+J does not significantly distort the geometry of Cu<sub>2</sub>O that is already predicted well by PBE.

The band-structure of DFT+U+J is qualitatively quite similar to the PBE one near the CBM and valence band maximum (VBM), as can be seen by a comparison of Fig. 6c. and Fig. 6d. However, the DFT+U+J functional does result in the opening of a ‘second gap’ in the valence band that is not present in the PBE band-structure, which starts 4.2 eV below the VBM and has a gap width of 2.2 eV. Such second gaps can be of interest for photovoltaic and other optoelectronic functionalities[85,86]. A previous quasiparticle G<sub>0</sub>W<sub>0</sub> study[17] shows a dip to zero or near-zero DOS at around the level predicted here for the second gap, but it is significantly less wide (<0.5 eV) than that found in this study. PES results do not seem to readily support the existence of such a gap[87]. This suggests that the second gap found using DFT+U+J may be either overestimated in magnitude, or the gap finding may be entirely erroneous. Ref. [88] indicates that the hybrid functional HSE06 does not predict this feature in Cu<sub>2</sub>O. The effective masses, shown in Fig. 6e, do not change substantially with the various tested functionals. The largest deviation occurs for DFT+U applied to metal only, where the  $m_e^*$  is about half of the PBE value.

### 3.6 Wurtzite ZnO results

Previous attempts at applying the linear response methodology to calculate the Hubbard U for Zn 3d orbitals in ZnO have encountered great difficulties, with researchers encountering either excessively high calculated U parameters[23,28] or numerical instability[29,30]. We have found that the almost perfectly fully filled Zn 3d orbitals require the applied perturbation to be increased by an order of magnitude in order to produce a sufficient change in occupancy level to overcome the numerical noise of the simulation. However, this unsurprisingly results in a response that is nonlinear. U and J values for these nonlinear responses can, in principle, still be estimated by taking the slope at zero perturbation of a good parabolic fit to the response curve. We found the resulting U and J values to be very high, with a 5x5x5 supercell calculation yielding the remarkable values of 83.7 eV for U and 9.3 eV for J. A DFT+U+J bandgap of 6.35 eV was calculated with these values, reflecting a saturating effect on the band-gap when the corrections are applied to a subset of orbitals. This is more than 3eV higher than the experimental gap.

It has been shown that DFT+U based modelling can be improved by applying U corrections to the 4s orbitals of certain transition metal systems.[29] This motivated us to calculate the linear response parameters of the Zn 4s subspaces, which is more relevant to the character of the band edges than the Zn 3d ones, particularly at the conduction band edge. For this it was necessary to change the PWscf source code trivially on a few lines, so that the desired angular momentum was selected. The charge response of the partially filled 4s subspace is much better behaved, and linear response can be readily extracted for the same perturbation range as for the four

prior materials, yielding U and J values that are much more plausible, as shown in Table 7. These values (for the largest supercell) were used for our evaluation.

**Table 7: Convergence of calculated U and J parameters for Zn 4s and O 2p subspaces in cubic ZnO with different supercell sizes and k-point grids.**

Supercell size	k-points	Zn U (eV)	Zn J (eV)	O U (eV)	O J (eV)
unit cell	6x6x6	1.753	0.953	19.293	3.910
2x2x2	$\Gamma$ -point	1.404	0.824	19.641	3.296
2x2x2	2x2x2	1.765	0.988	23.189	3.911
3x3x3	$\Gamma$ -point	1.743	0.993	22.540	3.871
3x3x3	2x2x2	1.795	1.072	23.428	3.954
4x4x4	$\Gamma$ -point	1.820	1.092	23.325	3.906
5x5x5	$\Gamma$ -point	1.815	1.066	23.325	3.906

Fig. 7a. shows the bandgap comparison for ZnO. The experimental bandgap is 3.44 eV[89]. Hybrid functionals consistently underestimate this gap, with the HSE06 average being 0.97 eV below experiment and PBE0 having a smaller error of 0.25 eV. Bare PBE drastically underestimates the gap, by 2.70 eV. Interestingly, applying the DFT+U correction to the Zn 4s orbitals alone actually makes the band-gap smaller, with the resulting error increasing to 3.11 eV. This is rectified by applying corrections to the O atoms as well, and the DFT+U (all atoms) method produces a band-gap that actually outperforms HSE06 as assessed from the literature, with an overcorrection of 0.63 eV. Both methods of applying J improve this slightly, with the 0.4 eV error of DFT+(U-J) making it the best performing of the PBE-based methods in this instance. The DFT+U+J functional gives a very close result to this, however, with an overestimation of 0.42 eV.

Fig. 7b. shows the effect of U correction on crystallographic geometry. The Zn 4s correction alone has almost no effect on the geometry. Applying U to the O atoms using either the DFT+U (all atoms) or DFT+(U-J) methods results in a shrinking of axis and bond lengths that overcorrects PBE somewhat. This still gives a lower geometric error overall than uncorrected PBE. The DFT+U+J method increase the error slightly, but it is still lower than that of PBE. This indicates that neither the unconventional choice of Zn 4s orbitals to define the subspaces targeted for correction, nor the somewhat high-seeming calculated O 2p U values, result in ionic geometry distortion. In fact, the geometry is improved with respect to that of PBE.

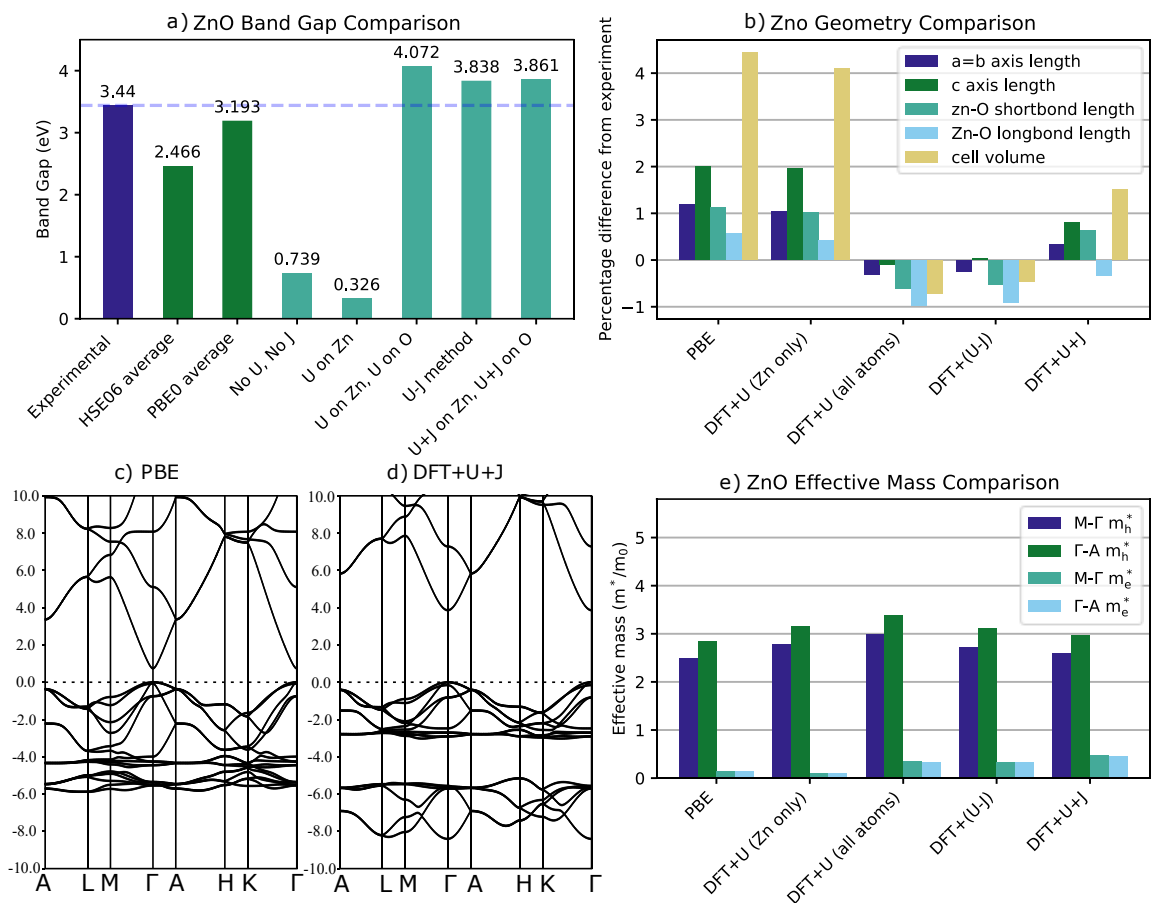


**Fig. 7. Full comparison of methodology choice effect on ZnO properties with corrections applied to 4s orbitals of Zn and 2p orbitals of O, showing the a) effect on band-gaps compared to experiment,[90] HSE06,[89,91-94] and PBE0[89,92,94]. b) geometric property differences with respect to experimental values. c) band-structure for PBE. d) band-structure for DFT+U+J. e) effective mass of along selected directions.**

A comparison of Fig. 7c. and Fig. 7d. indicates that the introduction of U and J introduces a second gap within the valence band that is not present in the bare PBE calculation, which starts at 3.0 eV below the VBM and has a gap width of 2.1 eV. This opening of this second gap has also been observed in some other DFT+U studies[95,96], some quasiparticle GW calculations by Kotani *et al.*[97] and in XPS data[98], although in general these second gaps appear to be much less wide than is seen here (<1eV). In contrast, most uncorrected GGA band-structures do not have a second gap[96,99], and the second gap similarly does not appear to be present in some HSE06 studies[89,91]. The effective mass of holes remains largely unchanged between methods, as can be seen in Fig. 7e. The effective mass of electrons, on the other hand, is very substantially increased multiplicatively.

### 3.7 Trends across the material test set

Table 8 summarizes the effect of the various corrective functionals on the band-gap for the materials investigated. Uncorrected PBE underestimates the bandgap of all materials by a significant degree, ranging from 27% for HfO<sub>2</sub> to 79% for ZnO. Applying DFT+U to the metal atoms alone increases the bandgap only slightly for each material except for ZnO (with 4s orbital subspaces targeted), where it actually makes the bandgap less accurate.

**Table 8: Evaluation of theoretical band-gap accuracy across five chemically diverse non-spin-polarized transition-metal oxides, using a variety of first-principles functionals derived from PBE and incorporating corrective Hubbard U and Hund’s exchange coupling J parameters, alongside HSE06 and PBE0 hybrid functional values based on available literature.**

Functional	Band-gap error with respect to experiment (%)					RMS error
	TiO <sub>2</sub>	ZrO <sub>2</sub>	HfO <sub>2</sub>	Cu <sub>2</sub> O	ZnO	
PBE	-39	-35	-27	-79	-79	52
DFT+U (metal only)	-33	-32	-25	-65	-90	49
DFT+U (all atoms)	26	38	58	48	18	38
DFT+(U-J)	13	24	42	23	12	23
DFT+U+J	-8	0	10	-23	13	11
HSE06 average	7	-9	-2	-11	-28	11
PBE0 average	30	11	13	14	-7	15

When the U is applied to both the metal and O atoms, an overestimation of the bandgap occurs in all five materials, with the largest by percentage occurring in HfO<sub>2</sub>. Using the DFT+(U-J) functional to scale down the effective U improves this slightly, but this still overestimates the gap for all materials.

The most comprehensive technique tested, that of applying both U and explicit unlike-spin J corrections in DFT+U+J, gives rise to a moderate overestimation of the bandgap for the 5d metal-oxide HfO<sub>2</sub> and the arguably marginal transition-metal oxide ZnO, a similar underestimation of the bandgap for the 3d metal-oxide Cu<sub>2</sub>O and TiO<sub>2</sub>, and the correct value within the experimental uncertainty for the 4d metal ZrO<sub>2</sub>. At least for the titanium Group 4 metal-oxides, the 4d pseudoatomic orbitals for PBE thus appear to represent a ‘goldilocks zone’ where the population analysis happens to be well suited to the assumptions underpinning DFT+U type methods. This conclusion might not be transferable to other periodic table groups, or other underlying functionals, we hasten to emphasize.

Meanwhile, the literature indicates that HSE06 slightly underestimates the gap on a root-mean squared (RMS) average basis, and that PBE0 overestimates it. The RMS error of first-principles DFT+U+J is 11%, which is lower than that of all of the other PBE-derived functionals, lower than that of PBE0 from literature, and equal to that of HSE06 values from the literature. This



demonstrates the DFT+U+J can provide band-gap accuracy comparable to hybrid functionals, and typically at a small fraction of the computational cost after the parameters are computed.

Table 9 shows a similar comparison of the effect of U and J on the crystallographic unit cell volume of each material. It can be seen that DFT+U applied to only the metal increases the volumetric error for every material except ZnO, and that it has the highest error of all the methods investigated. However, once the U correction is applied to the O atoms on the same footing as the metal atoms, the volumetric error drops to below that of regular PBE. This remains the case when J is applied using either of the functionals tested. The best performing functional for the lattice volume within this test set is DFT+(U-J), but the full DFT+U+J functional still provides a lower error than PBE. This demonstrates that accurate bandgaps do not need to come at the expense of spurious lattice distortion, as has previously been found in several studies[18-20], the key evidently being to correct the ligand band-edges subspaces (oxygen 2p in this study) on the same footing as the metal ones.

**Table 9: Comparison of accuracy of simulated volume across all five materials for each methodology of applying U and J corrections.**

Functional	Unit cell volume error with respect to experiment (%)					RMS error
	TiO <sub>2</sub>	ZrO <sub>2</sub>	HfO <sub>2</sub>	Cu <sub>2</sub> O	ZnO	
PBE	2.81	2.60	1.60	3.37	4.45	2.96
DFT+U (metal only)	4.60	3.47	2.02	10.52	4.11	4.94
DFT+U (all atoms)	0.77	0.68	-0.47	6.50	-0.72	1.83
DFT+(U-J)	0.96	0.66	-0.40	5.54	-0.42	1.59
DFT+U+J	2.59	2.30	1.21	3.95	1.60	2.33

Table 10 shows the difference in valence bandwidth between uncorrected PBE and DFT+U+J. The DFT+U+J functional, for the materials and subspace choices selected, consistently either stretches the valence bandwidth, or split it into two separate bands, predicting a “second gap” in CuO and ZnO. The appearance of a second gap in the valence band is a qualitative distinction that seems to feature in available many-body perturbation theory calculations for the Cu<sub>2</sub>O and ZnO band-structures, yet seems to be predicted by few if any DFT simulations except those of DFT+U or self-interaction correction type[17,89,90,95,96].

**Table 10: Comparison of valence bandwidths calculated using PBE and first-principles DFT+U+J constructed on the basis of PBE and PBE pseudoatomic orbitals.**

Technique	Valence bandwidth (eV)						
	TiO <sub>2</sub>	ZrO <sub>2</sub>	HfO <sub>2</sub>	Cu <sub>2</sub> O 1st band	Cu <sub>2</sub> O 2nd band	ZnO 1st band	ZnO 2nd band
PBE	5.63	4.91	5.50	7.08	n/a	5.88	n/a
DFT+U+J	6.31	5.92	6.83	4.19	3.23	3.03	3.25

## 4. Conclusion

In this study the use of linear response DFT+U+J was investigated as a means to accurately model closed-shell metal oxide bandgaps using unmodified, widely available plane-wave DFT software. It was demonstrated that Hund's coupling J parameters can be calculated successfully from first-principles using the familiar SCF linear-response formalism. The " $\gamma$ -method" was extended and verified within the SCF linear-response formalism, which allows for simultaneously calculating U and J in ultimately non-spin-polarized systems. This essentially makes the J a cost-free by-product of a U calculation.

Several corrective functionals incorporating Hubbard U and Hund's J corrections were evaluated in detail on a chemically diverse test set made up of TiO<sub>2</sub>, ZrO<sub>2</sub>, HfO<sub>2</sub>, Cu<sub>2</sub>O and ZnO. The fundamental bandgap, crystallographic geometry, and carrier effective masses were highlighted. It was shown that DFT+U+J (applied to both metal and O orbitals on the same footing) was overall the most successful functional for modelling the bandgap among those tested. First-principles DFT+U+J yielded the same root-mean-squared band-gap error as the popular, but much more computationally demanding and poorly-scaling hybrid functional HSE06.

Successful, or at least state-of-the-art level band-gap prediction, does not come at the cost of spurious crystallographic geometry distortion, as has been found in many previous DFT+U studies. The key difference in the present work being that the errors within the oxygen 2p subspaces were measured and corrected on the same footing as in the metal nd ones. In fact, the cell volumes predicted by DFT+U+J simulations were more accurate than those of standard PBE. Similarly, the effect on effective mass and band-structure tended to be small, although the bandwidth of the valence band was generally increased and a splitting of the valence band into two sub-bands was observed in the late transition-metal oxides Cu<sub>2</sub>O and ZnO.

Overall, DFT+U+J was found to be a highly viable method, which can be used easily within the widely available package Quantum Espresso. Moreover, it can be easily introduced into any DFT+U code, and no software modification at all is necessary if restricting its application to ultimately non-spin-polarized systems. We anticipate that the more widespread adoption of Hund's coupling J comprising corrective functionals, as a means to strengthen exchange effects locally at very low computational cost, could significantly improve the reliability of future materials discovery projects, while minimizing their environmental and financial footprint. Future research in this area could, e.g., examine the applicability of the methodology presented in this work to spin-polarized oxides, in which case Eqs. (9,10), not the  $\gamma$ -method, are required.

## Acknowledgements

This publication has emanated from research supported in part by a research grant from Science Foundation Ireland (SFI) and is co-funded under the European Regional Development Fund under Prime Award Number 12/RC/2278\_P2. We also acknowledge Trinity College Dublin Research IT and the DJEI/DES/SFI/HEA Irish Centre for High-End Computing (ICHEC) for the provision of computational facilities and support. Calculations were performed using the

Kay cluster at ICHEC and using three different clusters maintained by the Trinity Centre for High Performance Computing, the clusters Lonsdale, Kelvin and Boyle being funded by grants, respectively, from SFI, The Higher Education Authority through its PRTL program, and the European Research Council and SFI.

We are pleased to acknowledge financial support from Intel Corporation and insightful discussions and guidance from Justin Weber and Karthik Krishnaswamy. DDO'R wishes to thank and acknowledge Edward B. Linscott, Christoph Wolf, Carsten A. Ullrich, and Okan K. Orhan for prior discussions that encouraged a detailed study into calculating Hund's J using a self-consistent field DFT code.

## Appendix I: Results tables

Table 2 in section 3.1 demonstrated that the  $\gamma$ -method introduced in section 2.3 gave the same results as separate  $\alpha$ -for-U and  $\beta$ -for-J self-consistent field linear-response calculations for TiO<sub>2</sub>. Table 11 below summarizes similar tests for the other four materials. In all cases the difference between calculated values is very small, indicating that the  $\gamma$ -method is accurate for each material.

**Table 11 Demonstration that the U and J values calculated for ZrO<sub>2</sub>, HfO<sub>2</sub>, Cu<sub>2</sub>O and ZnO with separate  $\alpha$  and  $\beta$  linear response calculations and with the  $\gamma$ -method enabling simultaneous U and J calculation, are near-identical.**

Material	Parameter	$\alpha$ and $\beta$ method (eV)	$\gamma$ -method (eV)	Difference (eV)	Difference (%)
ZrO <sub>2</sub>	Zr U	1.728	1.724	-3.943E-03	-0.228
	Zr J	0.344	0.346	1.806E-03	0.525
	O U	14.187	14.126	-6.082E-02	-0.429
	O J	2.340	2.342	1.832E-03	0.078
HfO <sub>2</sub>	Hf U	1.440	1.442	1.496E-03	0.104
	Hf J	0.328	0.327	-1.225E-03	-0.373
	O U	17.939	17.875	-6.469E-02	-0.361
	O J	3.162	3.139	-2.371E-02	-0.750
Cu <sub>2</sub> O	Cu U	12.112	12.165	5.287E-02	0.436
	Cu J	1.978	1.980	2.095E-03	0.106
	O U	19.225	19.286	6.135E-02	0.319
	O J	3.259	3.250	-8.425E-03	-0.259
ZnO	Zn U	1.751	1.753	2.044E-03	0.117
	Zn J	0.978	0.953	-2.478E-02	-2.535
	O U	19.312	19.293	-1.936E-02	-0.100
	O J	4.006	3.910	-9.503E-02	-2.372

## References

- [1] A. Seidl, A. Görling, P. Vogl, J. A. Majewski, and M. Levy, Physical Review B **53**, 3764 (1996).

- [2] J. Heyd, G. E. Scuseria, and M. Ernzerhof, *The Journal of chemical physics* **118**, 8207 (2003).
- [3] A. V. Krukau, O. A. Vydrov, A. F. Izmaylov, and G. E. Scuseria, *The Journal of Chemical Physics* **125**, 224106 (2006).
- [4] C. Adamo and V. Barone, *The Journal of Chemical Physics* **110**, 6158 (1999).
- [5] B. G. Janesko, *Chemical Society Reviews* **50**, 8470 (2021).
- [6] B. Himmetoglu, A. Floris, S. De Gironcoli, and M. Cococcioni, *International Journal of Quantum Chemistry* **114**, 14 (2014).
- [7] M. R. Pederson, A. Ruzsinszky, and J. P. Perdew, *The Journal of Chemical Physics* **140**, 121103 (2014).
- [8] J. L. Bao, L. Gagliardi, and D. G. Truhlar, *The Journal of Physical Chemistry Letters* **9**, 2353 (2018).
- [9] I. Timrov, N. Marzari, and M. Cococcioni, *Physical Review B* **103**, 045141 (2021).
- [10] V. I. Anisimov, J. Zaanen, and O. K. Andersen, *Physical Review B* **44**, 943 (1991).
- [11] V. I. Anisimov, I. Solovyev, M. Korotin, M. Czyżyk, and G. Sawatzky, *Physical Review B* **48**, 16929 (1993).
- [12] I. Solovyev, P. Dederichs, and V. Anisimov, *Physical Review B* **50**, 16861 (1994).
- [13] M. Cococcioni and S. De Gironcoli, *Physical Review B* **71**, 035105 (2005).
- [14] W. E. Pickett, S. C. Erwin, and E. C. Ethridge, *Physical Review B* **58**, 1201 (1998).
- [15] H. J. Kulik, M. Cococcioni, D. A. Scherlis, and N. Marzari, *Physical Review Letters* **97**, 103001 (2006).
- [16] X. Han and G. Shao, *The Journal of Physical Chemistry C* **115**, 8274 (2011).
- [17] L. Y. Isseroff and E. A. Carter, *Physical Review B* **85**, 235142 (2012).
- [18] E. S. Goh, J. W. Mah, and T. L. Yoon, *Computational Materials Science* **138**, 111 (2017).
- [19] E. German, R. Faccio, and A. W. Mombrú, *Journal of Physics Communications* **1**, 055006 (2017).
- [20] A. Janotti, D. Segev, and C. G. Van de Walle, *Physical Review B* **74**, 045202 (2006).
- [21] D. Gupta, S. R. Meher, N. Illyaskutty, and Z. C. Alex, *Journal of Alloys and Compounds* **743**, 737 (2018).

- [22] K. Harun, M. K. Yaakob, M. F. Mohamad Taib, B. Sahraoui, Z. A. Ahmad, and A. A. Mohamad, *Materials Research Express* **4**, 085908 (2017).
- [23] E. M. Flores, M. L. Moreira, and M. J. Piotrowski, *The Journal of Physical Chemistry A* **124**, 3778 (2020).
- [24] S. A. Tolba and N. K. Allam, *Scientific Reports* **9**, 10159 (2019).
- [25] G. Mattioli, P. Alippi, F. Filippone, R. Caminiti, and A. Amore Bonapasta, *The Journal of Physical Chemistry C* **114**, 21694 (2010).
- [26] B. J. Morgan and G. W. Watson, *Physical Review B* **80**, 233102 (2009).
- [27] N. E. Kirchner-Hall, W. Zhao, Y. Xiong, I. Timrov, and I. Dabo, arXiv preprint arXiv:2102.04636 (2021).
- [28] K. Yu and E. A. Carter, *The Journal of Chemical Physics* **140**, 121105 (2014).
- [29] H. J. Kulik and N. Marzari, *The Journal of Chemical Physics* **133**, 114103 (2010).
- [30] S.-J. Hu, S.-S. Yan, M.-W. Zhao, and L.-M. Mei, *Physical Review B* **73**, 245205 (2006).
- [31] A. Georges, L. D. Medici, and J. Mravlje, *Annual Review of Condensed Matter Physics* **4**, 137 (2013).
- [32] S. L. Dudarev, G. A. Botton, S. Y. Savrasov, C. J. Humphreys, and A. P. Sutton, *Physical Review B* **57**, 1505 (1998).
- [33] M. Shishkin and H. Sato, *The Journal of Chemical Physics* **154**, 114709 (2021).
- [34] D. Soler-Polo, J. Ortega, and F. Flores, *Journal of Physics: Condensed Matter* **33**, 425604 (2021).
- [35] B. Himmetoglu, R. M. Wentzcovitch, and M. Cococcioni, *Physical Review B* **84**, 115108 (2011).
- [36] E. B. Linscott, D. J. Cole, M. C. Payne, and D. D. O'Regan, *Physical Review B* **98**, 235157 (2018).
- [37] O. K. Orhan and D. D. O'Regan, *Physical Review B* **101**, 245137 (2020).
- [38] P. Giannozzi *et al.*, *Journal of Physics: Condensed Matter* **21**, 395502 (2009).
- [39] P. Giannozzi *et al.*, *Journal of Physics: Condensed Matter* **29**, 465901 (2017).
- [40] J. C. A. Prentice *et al.*, *The Journal of Chemical Physics* **152**, 174111 (2020).
- [41] J. P. Perdew, K. Burke, and M. Ernzerhof, *Physical review letters* **77**, 3865 (1996).
- [42] S. Dudarev, P. Liu, D. Andersson, C. Stanek, T. Ozaki, and C. Franchini, *Physical Review Materials* **3**, 083802 (2019).

- [43] D. D. O'Regan and G. Teobaldi, *Physical Review B* **94**, 035159 (2016).
- [44] A. Dal Corso, *Computational Materials Science* **95**, 337 (2014).
- [45] H. J. Monkhorst and J. D. Pack, *Physical review B* **13**, 5188 (1976).
- [46] L. A. Agapito, S. Curtarolo, and M. Buongiorno Nardelli, *Physical Review X* **5**, 011006 (2015).
- [47] S.-G. Park, B. Magyari-Köpe, and Y. Nishi, *Physical Review B* **82**, 115109 (2010).
- [48] M. Kick, K. Reuter, and H. Oberhofer, *Journal of Chemical Theory and Computation* **15**, 1705 (2019).
- [49] J. Pascual, J. Camassel, and H. Mathieu, *Physical Review B* **18**, 5606 (1978).
- [50] A. Amtout and R. Leonelli, *Physical Review B* **51**, 6842 (1995).
- [51] F. Labat, P. Baranek, C. Domain, C. Minot, and C. Adamo, *The Journal of Chemical Physics* **126**, 154703 (2007).
- [52] R. A. Evarestov and Y. F. Zhukovskii, *Surface Science* **608**, 226 (2013).
- [53] W. Kang and M. S. Hybertsen, *Physical Review B* **82**, 085203 (2010).
- [54] M. Landmann, E. Rauls, and W. Schmidt, *Journal of physics: condensed matter* **24**, 195503 (2012).
- [55] Y. Luo, A. Benali, L. Shulenburger, J. T. Krogel, O. Heinonen, and P. R. Kent, *New Journal of Physics* **18**, 113049 (2016).
- [56] H. Chen, X. Li, R. Wan, S. Kao-Walter, and Y. Lei, *Chemical Physics* **501**, 60 (2018).
- [57] P. Deák, B. Aradi, and T. Frauenheim, *Physical Review B* **92**, 045204 (2015).
- [58] H. P. R. Frederikse, *Journal of Applied Physics* **32**, 2211 (1961).
- [59] F. A. Grant, *Reviews of Modern Physics* **31**, 646 (1959).
- [60] H. Wu, Y. Duan, K. Liu, D. Lv, L. Qin, L. Shi, and G. Tang, *Journal of Alloys and Compounds* **645**, 352 (2015).
- [61] F. Opoku and P. P. Govender, *Materials Chemistry and Physics* **224**, 107 (2019).
- [62] H. Yildirim and R. Pachter, *ACS Applied Electronic Materials* **1**, 467 (2019).
- [63] A. Sinhamahapatra, J.-P. Jeon, J. Kang, B. Han, and J.-S. Yu, *Scientific Reports* **6**, 27218 (2016).
- [64] J.-H. Hur, S. Park, and U. I. Chung, *Journal of Applied Physics* **112**, 113719 (2012).

- [65] C. Ricca, A. Ringuedé, M. Cassir, C. Adamo, and F. Labat, *Journal of Computational Chemistry* **36**, 9 (2015).
- [66] M. Grüning, R. Shaltaf, and G.-M. Rignanese, *Physical Review B* **81**, 035330 (2010).
- [67] H. Jiang, R. I. Gomez-Abal, P. Rinke, and M. Scheffler, *Physical Review B* **81**, 085119 (2010).
- [68] B. Králik, E. K. Chang, and S. G. Louie, *Physical Review B* **57**, 7027 (1998).
- [69] E. Bersch, S. Rangan, R. A. Bartynski, E. Garfunkel, and E. Vescovo, *Physical Review B* **78**, 085114 (2008).
- [70] S. Sayan *et al.*, *Journal of Applied Physics* **96**, 7485 (2004).
- [71] H.-P. Komsa, P. Broqvist, and A. Pasquarello, *Physical Review B* **81**, 205118 (2010).
- [72] W. Zhang and Z. F. Hou, *physica status solidi (b)* **250**, 352 (2013).
- [73] S. R. Bradley, UCL (University College London), 2016.
- [74] J. H. Skone, M. Govoni, and G. Galli, *Physical Review B* **89**, 195112 (2014).
- [75] L. Qi-Jun, Z. Ning-Chao, L. Fu-Sheng, and L. Zheng-Tang, *Chinese Physics B* **23**, 047101 (2014).
- [76] B. Sklénard, A. Dragoni, F. Triozon, and V. Olevano, *Applied Physics Letters* **113**, 172903 (2018).
- [77] W. Chen and A. Pasquarello, *Physical Review B* **86**, 035134 (2012).
- [78] S. Brahms, S. Nikitine, and J. Dahl, *Physics Letters* **22**, 31 (1966).
- [79] I. S. Brandt, M. A. Tumelero, C. A. Martins, C. C. Plá Cid, R. Faccio, and A. A. Pasa, *Journal of Applied Physics* **123**, 161412 (2018).
- [80] M. Benaissa, H. S. Abdelkader, and G. Merad, *Optik* **207**, 164440 (2020).
- [81] Q. Bai, W. Wang, Q. Zhang, and M. Tao, *Journal of Applied Physics* **111**, 023709 (2012).
- [82] J. Linnera and A. J. Karttunen, *Physical Review B* **96**, 014304 (2017).
- [83] A. Visibile, R. B. Wang, A. Vertova, S. Rondinini, A. Minguzzi, E. Ahlberg, and M. Busch, *Chemistry of Materials* **31**, 4787 (2019).
- [84] X.-G. Yan, L. Xu, W.-Q. Huang, G.-F. Huang, Z.-M. Yang, S.-Q. Zhan, and J.-P. Long, *Materials Science in Semiconductor Processing* **23**, 34 (2014).
- [85] O. Mryasov and A. Freeman, *Physical Review B* **64**, 233111 (2001).
- [86] V.-A. Ha, D. Waroquiers, G.-M. Rignanese, and G. Hautier, *Applied Physics Letters* **108**, 201902 (2016).

- [87] A. Önsten, M. Månsson, T. Claesson, T. Muro, T. Matsushita, T. Nakamura, T. Kinoshita, U. O. Karlsson, and O. Tjernberg, *Physical Review B* **76**, 115127 (2007).
- [88] M. Heinemann, B. Eifert, and C. Heiliger, *Physical Review B* **87**, 115111 (2013).
- [89] K. Bashyal, C. K. Pyles, S. Afroosheh, A. Lamichhane, and A. T. Zayak, *Journal of Physics: Condensed Matter* **30**, 065501 (2018).
- [90] D. Vogel, P. Krüger, and J. Pollmann, *Physical Review B* **54**, 5495 (1996).
- [91] J.-H. Luo, Q. Liu, L.-N. Yang, Z.-Z. Sun, and Z.-S. Li, *Computational Materials Science* **82**, 70 (2014).
- [92] M. Gerosa, C. E. Bottani, L. Caramella, G. Onida, C. Di Valentin, and G. Pacchioni, *Physical Review B* **91**, 155201 (2015).
- [93] Q. Yan, P. Rinke, M. Winkelkemper, A. Qteish, D. Bimberg, M. Scheffler, and C. G. Van de Walle, *Semiconductor science and technology* **26**, 014037 (2010).
- [94] J. Yu, L. K. Wagner, and E. Ertekin, *Physical Review B* **95**, 075209 (2017).
- [95] P. Erhart, K. Albe, and A. Klein, *Physical Review B* **73**, 205203 (2006).
- [96] X. Ma, Y. Wu, Y. Lv, and Y. Zhu, *The Journal of Physical Chemistry C* **117**, 26029 (2013).
- [97] T. Kotani, M. Van Schilfgaarde, and S. V. Faleev, *Physical Review B* **76**, 165106 (2007).
- [98] P. D. C. King *et al.*, *Physical Review B* **79**, 205205 (2009).
- [99] H. Cao, P. Lu, N. Cai, X. Zhang, Z. Yu, T. Gao, and S. Wang, *Journal of Magnetism and Magnetic Materials* **352**, 66 (2014).